Confocal photoacoustic microscopy using a single multifunctional lens

Lei Xi,† Chaolong Song,† and Huabei Jiang*

Department of Biomedical Engineering, University of Florida, Gainesville, Florida 32611, USA
**Corresponding author: hjiang@bme.ufl.edu*

Received March 28, 2014; revised April 7, 2014; accepted April 26, 2014;
posted April 28, 2014 (Doc. ID 209018); published May 30, 2014

Photoacoustic microscopy (PAM) has remained one of the fastest developing biomedical imaging modalities in the past decade. The confocal strategy of optical illumination and acoustic detection is a way to boost the sensitivity of PAM. To achieve confocal PAM, current PAM systems utilize separate acoustic and optical converging devices, making the systems bulky and complicated. In this Letter, we demonstrate the use of a single-liquid lens to successfully achieve acoustic and optical confocal configuration for optical-resolution PAM (ORPAM). Using the lens with a numerical aperture of 0.43, we show that the resolution of the ORPAM system is 4.8 μm with a significantly improved sensitivity of acoustic detection. We also apply this compact ORPAM system to *in vivo* imaging of the vasculature of a rat ear.

OCIS codes: (110.5120) Photoacoustic imaging; (110.0180) Microscopy; (080.3630) Lenses.
http://dx.doi.org/10.1364/OL.39.003328

Photoacoustic microscopy (PAM) is probably the most rapidly developing photoacoustic imaging technique among all photoacoustic imaging modalities [1–3]. PAM is generally categorized into two submodalities depending on its resolving abilities: acoustic-resolution PAM (ARPAM) and optical-resolution PAM (ORPAM) [4]. Images in PAM are obtained by mechanically scanning either a focused transducer (ARPAM) or a confined laser beam (ORPAM). The acquired one-dimensional (1D) acoustic signals (A-lines) are backprojected directly to form a two-dimensional (2D) or three-dimensional (3D) image without the aid of any reconstruction algorithms. To enhance the sensitivity of PAM, acoustic and optical confocal strategy is commonly achieved with separate acoustic and optical converging strategies and complicated system configurations. For ARPAM, a conical lens and an optical condenser are commonly used to weakly focus the illumination beam, and complicated adjustments are required to coaxially overlap the optical focus with the ultrasonic focus. ORPAM systems usually employ both an acoustic lens and an objective lens to achieve acoustic and optical focus, and a special combiner that reflects/transmits acoustic waves and transmits/reflects optical beams to realize coaxial confocal configuration of optical illumination and acoustic detection [5–7]. Both configurations make the PAM systems complicated and experience-based, especially for ORPAM systems. Recently, we developed a liquid-based variable-focus lens to effectively achieve either acoustic diverging or converging, and evaluated it using both a photoacoustic tomography imaging system and an ARPAM imaging system [8,9]. This liquid lens has several advantages: (1) it has inherent low acoustic impedance that can effectively reduce the reflective loss of acoustic signals; (2) it has a tunable focal length that enables the axial adjustment of the acoustic focus without mechanical scanning; and (3) it is cheap and easily replaceable. Liquid-filled optical lenses have already been used widely and offer the potential to minimize and simplify the optical systems [10,11]. In principle, the liquid-filled acoustic and optical lenses perform a similar physical function based on the difference of the acoustic or optical refractive index between the internal and external liquids. Here, we propose the use of two different types of liquids but with the same relative acoustic and optical refractive index to achieve coaxial confocal configuration of optical illumination and acoustic detection. We use this new liquid lens to build a compact ORPAM imaging system and evaluate its performance with phantom and *in vivo* animal experiments.

Similar to most ORPAM imaging systems, as shown in Fig. 1, the visible laser beam (532 nm) generated by a Nd:YAG pulsed laser (Surelite I-20, Continuum) was first attenuated, then coupled into a single mode fiber (P1-460B-FC-1, Thorlabs) using two neutral-density filters and one objective lens. The whole imaging probe consisting of an optical collimator (F260FC-A, Thorlabs), a ring-shaped 5 MHz transducer (external diameter: 11 mm; internal diameter: 5 mm), and a liquid lens with a size of 11.5 mm in diameter was mounted on a 2D scanner. The photoacoustic signals captured were amplified (5072PR, Olympus), digitalized (NI5124, National Instruments), and stored in a computer. A beam splitter and an ultrafast photodiode were used to record the pulse fluctuation that was used to calibrate the imaging data. Figure 2 is the close view of the imaging probe shown by the red dashed rectangle in Fig. 1. The fabrication and evaluation of the liquid-based lens can be found in our previous publications [8,9]. As shown in the figure, the laser beam was first collimated by the

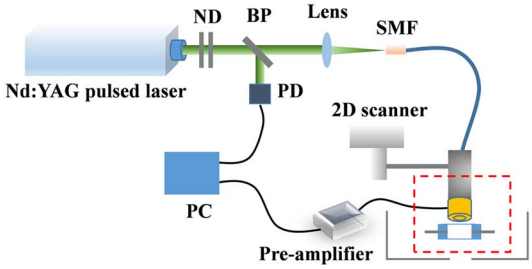

Fig. 1. Schematic of the ORPAM imaging system. ND, neutral-density filters; PD, photodiode; BP, beam splitter; SMF, single-mode fiber.

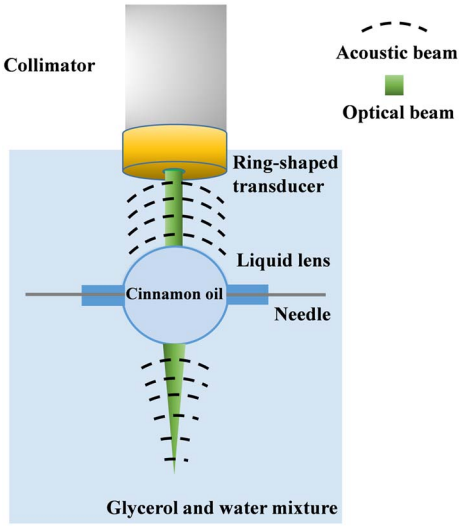

Fig. 2. Schematic of the compact ORPAM imaging probe.

optical collimator with an output size of 2.8 mm in diameter, and then focused by the liquid lens infused with cinnamon oil through a needle and tubing by a syringe pump (KDS 210, KD Scientific). A plastic holder was used to position both the ring-shaped transducer and the lens. The tank was filled with a mixture of glycerol and water.

Under the condition of a fully infused biconvex lens, both the optical and acoustic focal lengths can be formulated as [9,12,13]

$$f = \frac{r}{2 \times (n-1)}, \tag{1}$$

where r is the radius of the interface curvature and n is the optical/acoustic relative refractive index, which is calculated by the following equations:

$$n_{\text{optical}} = \frac{n_{\text{internal}}}{n_{\text{external}}}, \tag{2}$$

$$n_{\text{acoustic}} \frac{V_{\text{external}}}{V_{\text{internal}}}, \tag{3}$$

where n_{internal} and n_{external} represent, respectively, the optical refractive indexes of the internal and external liquids, and V_{internal} and V_{external} are, respectively, the sound velocities of the internal and external liquids. Coaxial confocal configuration of optical illumination and acoustic detection is possible if the internal liquid has a higher refractive index and a lower sound velocity compared with the external liquid. Cinnamon oil with an impressively high optical refractive index (1.63) and a modest sound velocity (1480 m/s) serves well as the internal liquid in the area of optical liquid lens and microfluidics. From our previous publication [8], we noted that pure glycerol has a higher sound velocity (1920 m/s) and a lower optical refractive index (1.47) compared with those of cinnamon oil. Hence, it is feasible to achieve acoustic and optical confocal by using cinnamon oil as the internal liquid and a mixture of glycerol and water as the external liquid.

In Fig. 3A, we have plotted the curves of acoustic (red) and optical (blue) relative refractive index versus the weight percentage of water in the mixture. Acoustic relative refractive index decreased and optical relative refractive index increased when the weight percentage of water increased. Both the optical and acoustic relative refractive indexes were 1.15 when the weight percentage of water was 42%. Given that the radius of the lens and the acoustic transducer was 5.5 mm, and the liquid lens was infused fully, the numerical aperture of the lens and the shortest focal length were determined to be 0.43 and 18 mm, respectively.

To capture light rays, a fluorescence dye Rhodamine B (Sigma-Aldrich, excitation wavelength = 540 nm, emission wavelength = 625 nm) was diluted in the mixture. Grayscale images were recorded with a CCD camera (Princeton Instruments). To characterize the acoustic converging ability of the lens, the transducer was driven by a pulser/receiver (5072PR, Olympus) to generate acoustic emission. A hydrophone (HGL-0200, ONDA) with a circular sensing area of 0.2 mm in diameter was scanned laterally to map the acoustic pressure distribution of the transducer. Figure 3B shows the optical rays and acoustic pressure distributions when the lens was flat and fully infused. We can see that the lens enabled coaxial acoustic and optical confocal configuration with a focal length of 19 mm. As we expected, the optical and pressure intensities were highly confined when the lens was infused fully. However, the focal length measured was slightly longer than the theoretical estimation since the alignment between the collimator/transducer and the lens was not optimal.

The 1D profile along the dashed white line across the acoustic focal point shown in Fig. 3B is given in Fig. 4A, and was used to estimate the size of the acoustic focus. The full width at half-maximum was found to be 0.7 mm, which was slightly larger than the theoretical estimation (0.6 mm) calculated by the following equation, due to misalignment of the transducer and the lens [14]:

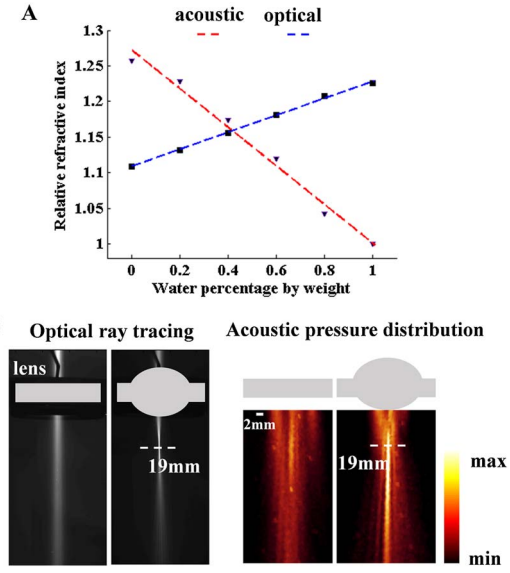

Fig. 3. A, acoustic and optical relative refractive index versus weight percentage of water in the mixture; B, optical rays and acoustic pressure distribution when the lens was flat and fully infused.

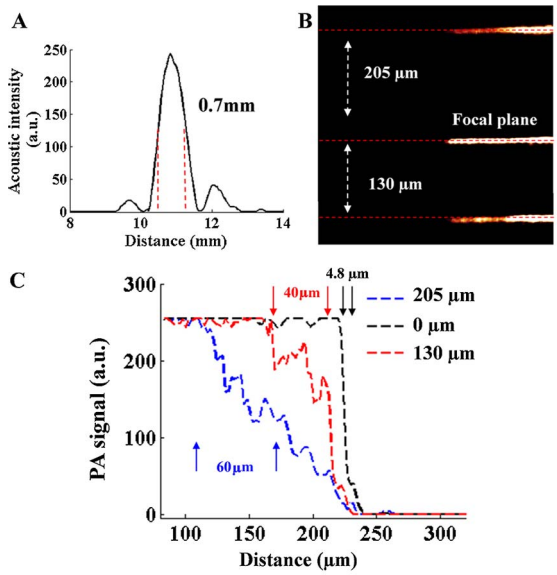

Fig. 4. A, 1D profile along the dashed white line across the acoustic focal point shown in Fig. 3B; B, B-scan images of the blade in the focal plane. 130 and 205 μm off the focal plane; C, 1D profile along the red dashed line shown in Fig. 4B.

$$\text{Resolutionn}_{(=6\text{ dB})} = \frac{1.028 \times f \times c}{F \times D}, \tag{4}$$

where f is the focal length, c is sound velocity, F is the central frequency, and D is the element diameter of the transducer.

We employed the edge spread function to estimate the lateral resolution of this imaging system. The shape edge of 10 blades was imaged. One B-scan image contained 200 A-lines with an interval step of 2.5 μm and a total of 100 B-scan images were obtained by performing axial scanning with a scanning step of 5 μm. Figure 4B shows the B-scan images when the blade was in the focal plane, and 130 and 205 μm off the focal plane. From the profiles given in Fig. 4C, we find that the resolution in the focal plane is 4.8 μm, and the resolutions in the out-of-focus planes are much poor (40 μm in the plane, 130 μm off the focal plane and 60 μm in the plane, 205 μm off the focal plane).

A human hair was embedded inside a tissue mimicking phantom with an absorption coefficient of 0.007 mm^{-1} and a reduced scattering coefficient of 1 mm^{-1} to evaluate the sensitivity of this imaging system with and without acoustic focused detection. In the first experiment, the mixture of glycerol and water served as the external liquid and enabled acoustic and optical confocal configuration. In the control experiment, pure water that enabled only optical converging was used. Maximum amplitude projection (MAP) images (Fig. 5A) and a quantitative comparison (Fig. 5B) show a significant improvement in sensitivity by using a confocal configuration.

In vivo experiments were carried out to demonstrate the potential biomedical application of this technique. A rat was kept motionless using a breathing anesthesia system and body temperature was maintained at 37°C with a temperature-controlling pad. The rat ears were depilated gently before tightly contacting the membrane-sealed imaging window at the bottom of the tank. All procedures were approved by the Institutional Animal

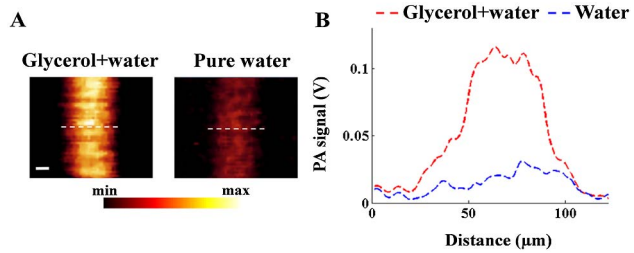

Fig. 5. A, MAP of human hair with and without acoustic focusing; B, 1D plots along the dashed lines in Fig. 5A. Scale bar: 20 μm.

Care and Use Committee (IACUC) at the University of Florida. The total raster scanning points was 200 along each transverse direction with an interval of 5 μm over a distance of 1 mm. The laser pulse energy after the lens was measured to be 100 nJ. The experimental time for a complete volumetric data collection was 40 min. After the data acquisition, the rat recovered fully without any observable laser damage. The microvasculature was imaged clearly as shown in Fig. 6A. The top image is a MAP along the axial direction and the bottom image is a selected cross-section image along the dashed white line in the MAP. Figure 6B shows a 3D pseudocolor visualization of the vasculature.

Laser damage and bleaching occur commonly when using a high-energy pulsed laser [15]. The focal fluence in the *in vivo* animal experiments was 550 mJ/cm^2 in water, which is still less than the damage threshold observed experimentally in small animals [16]. When the focal point was 130 μm below the tissue surface, the surface optical fluence was 8 mJ/cm^2, which is smaller than the American National Standards Institute (ANSI) safety limit (20 mJ/cm^2 in the visible wavelengths).

In summary, we have demonstrated the use of a single-liquid lens to realize coaxial optical illumination and acoustic detection confocal configuration in ORPAM. Phantom and *in vivo* experiments were carried out to evaluate the performance of the lens. We note that the application of this lens is not limited to ORPAM systems. If we use an optical fiber bundle instead of a single-mode optical fiber, we can build an ARPAM imaging system with a weakly confocal configuration of optical illumination and acoustic detection using a single-liquid lens. In addition, the variable focal length of the lens enables us to easily integrate fluorescence confocal microscopy with PAM. We also recognize that the central frequency

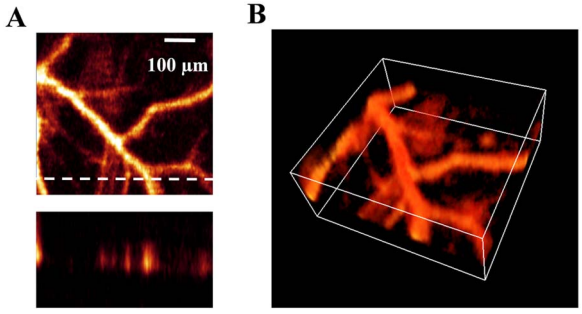

Fig. 6. A, A MAP image (top) and a selected B-scan image (bottom) of the rat ear; B, volumetric rendering of the vasculature of the imaged rat ear.

of the current ring-shaped transducer is not high, which led to a relatively poor axial resolution and a low sensitivity to capillaries. In addition, the inner diameter of the transducer is larger than the laser beam. A high-frequency ring-shaped transducer with a small inner diameter can significantly improve the sensitivity and axial resolution of this imaging system. Finally, a fast laser can significantly reduce the data acquisition time.

This research was supported in part by an NIH grant (CA 161384) and the J. Crayton Pruitt Family endowment fund.

†These authors contributed equally to this work.

References

1. P. Beard, Interface Focus **1**, 602 (2011).
2. H. F. Zhang, K. Maslov, G. Stoica, and L. V. Wang, Nat. Biotechnol. **24**, 848 (2006).
3. L. Xi, L. Zhou, and H. Jiang, Appl. Phys. Lett. **101**, 013702 (2012).
4. L. V. Wang and S. Hu, Science **335**, 1458 (2012).
5. X. Yang, X. Cai, K. Maslov, L. V. Wang, and Q. Luo, Chin. Opt. Lett. **8**, 609 (2010).
6. K. Maslov, H. F. Zhang, S. Hu, and L. V. Wang, Opt. Lett. **33**, 929 (2008).
7. Y. Yuan, S. Yang, and D. Xing, Appl. Phys. Lett. **100**, 023702 (2012).
8. C. Song, L. Xi, and H. Jiang, Opt. Lett. **38**, 2930 (2013).
9. C. Song, L. Xi, and H. Jiang, J. Appl. Phys. **114**, 194703 (2013).
10. G. C. Knollman, J. L. S. Bellin, and J. L. Weaver, J. Acoust. Soc. Am. **49**, 253 (1971).
11. N. Sugiura and S. Morita, Appl. Opt. **32**, 4181 (1993).
12. C. Song, N. T. Nguyen, S. H. Tan, and A. K. Asundi, Lab Chip **9**, 1178 (2009).
13. C. Song, N. T. Nguyen, S. H. Tan, and A. K. Asundi, Microfluid. Nanofluid. **9**, 889 (2010).
14. K. H. Song and L. V. Wang, J. Biomed. Opt. **12**, 060503 (2007).
15. J. T. Walsh, T. J. Flotte, and T. F. Deutsch, Lasers Surg. Med. **9**, 314 (1989).
16. V. P. Zharov, E. I. Galanzha, E. V. Shashkov, N. G. Khlebtsov, and V. V. Tuchin, Opt. Lett. **31**, 3623 (2006).